TU Delft

Delft University of Technology

Surface-micromachined Silicon Carbide Pirani Gauges for Harsh Environments

Mo, Jiarui; Middelburg, Luke M.; Morana, Bruno; Zeijl, H.W. Van; Vollebregt, Sten; Zhang, GuoQi

DOI
10.1109/JSEN.2020.3019711

Publication date
2021

Document Version
Final published version

Published in
IEEE Sensors Journal

Citation (APA)
Mo, J., Middelburg, L. M., Morana, B., Zeijl, H. W. V., Vollebregt, S., & Zhang, G. (2021). Surface-micromachined Silicon Carbide Pirani Gauges for Harsh Environments. *IEEE Sensors Journal*, *21*(2), 1350-1358. Article 9178352. https://doi.org/10.1109/JSEN.2020.3019711

Important note
To cite this publication, please use the final published version (if applicable).
Please check the document version above.

Copyright
Other than for strictly personal use, it is not permitted to download, forward or distribute the text or part of it, without the consent of the author(s) and/or copyright holder(s), unless the work is under an open content license such as Creative Commons.

Takedown policy
Please contact us and provide details if you believe this document breaches copyrights.
We will remove access to the work immediately and investigate your claim.

This work is downloaded from Delft University of Technology.
For technical reasons the number of authors shown on this cover page is limited to a maximum of 10.

Green Open Access added to TU Delft Institutional Repository

'You share, we take care!' - Taverne project

https://www.openaccess.nl/en/you-share-we-take-care

Otherwise as indicated in the copyright section: the publisher is the copyright holder of this work and the author uses the Dutch legislation to make this work public.

Surface-Micromachined Silicon Carbide Pirani Gauges for Harsh Environments

Jiarui Mo, Luke M. Middelburg, *Member, IEEE*, Bruno Morana, H. W. van Zeijl, *Member, IEEE*, Sten Vollebregt, *Senior Member, IEEE*, and Guoqi Zhang, *Fellow, IEEE*

***Abstract*—The application of pressure sensors in harsh environments is typically hindered by the stability of the material over long periods of time. This work focuses on the design and fabrication of surface micromachined Pirani gauges which are designed to be compatible with state-of-the-art Silicon Carbide CMOS technology. Such an integrated platform would boost harsh environment compatibility while reducing the required packaging complexity. An analytical model was derived describing the design variables of the Pirani gauges followed by Finite Element Analysis. The Pirani gauges were fabricated in a CMOS compatible cleanroom with a process employing only three masks, thus suitable for mass production. The SiC-based Pirani gauge is far more competitive than the traditional Si-based Pirani gauge in terms of endurance in high-temperature environments. From 25°C to 650°C, the gauge shows a reproducible response to pressure changes and has a maximum sensitivity of 17.63 Ω/Pa at room temperature, and of 1.23 Ω/Pa at 650°C. Additionally, some of the gauges were demonstrated to operate at temperatures up to 750°C.**

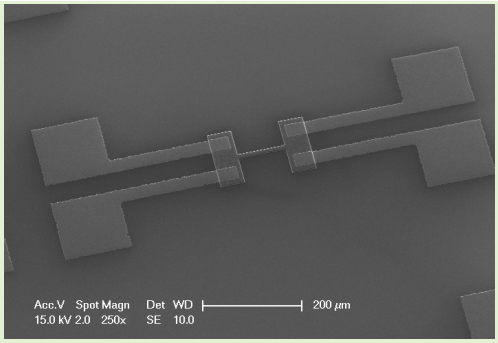

***Index Terms*—Pressure sensor, MEMS, harsh environments, vacuum gauge, silicon carbide, surface micromaching.**

I. Introduction

PRESSURE monitoring is an important topic for several industries, such as automotive, aerospace, and semiconductor. In terms of vacuum level monitoring, the Pirani gauge is, without doubt, one of the most popular choices for measuring rough and/or medium vacuum. Its success relies on its simple structure and the absence of moving parts. This results in excellent mechanical robustness and high reliability.

Not until recently, MEMS (micro-electro-mechanical systems) technology has been employed for the realization of silicon-based Pirani gauges. By leveraging on the mature silicon manufacturing technology, it is possible to transform conventional macroscopic pressure sensors into microfabricated devices. Miniaturized devices have advantages in terms of size, power consumption, and costs compared with conventional devices. Additionally, Si-based Pirani gauges can be integrated with a readout circuit to further reduce the size and enhance the reliability of the overall system. In 1991, Mastrangelo *et al.* fabricated a MEMS Pirani gauge based on poly-Si with an integrated on-chip circuitry able to process the sensing signal [1].

In the past decade, the improvement of the Pirani gauge is still ongoing. Santagata *et al.* optimized the traditional structure of a Pirani gauge by creating a tube-shaped device that resulted in improved stiffness and higher sensitivity [2]. Also, advanced materials have been introduced to build Pirani sensors. In 2013, Yu *et al.* employed dielectrophoretic (DEP) assembly technique to prepare a single-walled carbon nanotube Pirani gauge, which demonstrated an ultra-low power consumption (15 nW) and high sensitivity in a large dynamic range (0.8 to 80000 Pa) [3]. In 2018, the world first graphene-based Pirani gauge was designed by J. Romijn *et al.* The graphene-based Pirani gauge they fabricated has a 100 times smaller footprint than the existing Pirani gauge while maintaining a comparable sensitivity to the state-of-the-art microfabricated Pirani gauge [4].

In recent years, more scenarios require measurement systems to work in extremely high temperatures, demanding harsh environment compatible sensors. Application examples are, for instance, low pressure chemical vapor deposition furnaces, oil drilling, combustion monitoring, and the electronics for space exploration [5]. A variety of sensors are designed to fit the high-temperature application. Table I summarizes such progress in the last two decades.

Manuscript received June 29, 2020; revised August 10, 2020; accepted August 15, 2020. Date of publication August 26, 2020; date of current version December 16, 2020. The associate editor coordinating the review of this article and approving it for publication was Dr. Eui-Hyeok Yang. *(Corresponding author: Jiarui Mo.)*

The authors are with the Laboratory of Electronic Components, Technology, and Materials, Delft University of Technology, 2628 Delft, The Netherlands (e-mail: j.mo@tudelft.nl; l.m.middelburg@tudelft.nl; b.morana@tudelft.nl; h.w.vanzeijl@tudelft.nl; s.vollebregt@tudelft.nl; g.q.zhang@tudelft.nl).

Digital Object Identifier 10.1109/JSEN.2020.3019711

1558-1748 © 2020 EU

Authorized licensed use limited to: TU Delft Library. Downloaded on January 12,2021 at 12:43:38 UTC from IEEE Xplore. Restrictions apply.

TABLE I
SENSORS FOR THE HIGH-TEMPERATURE ENVIRONMENT IN THE RECENT 20 YEARS

Researcher [ref.]	Sensor type/Mechanism	Functional material	Max. operating temperature
D.J. Young et al. [6]	Capacitive pressure sensor	SiC	400°C
M. Werner et al. [7]	Piezoresistive pressure sensor	Diamond	170°C
S. Li et al. [8]	Piezoresistive pressure sensor	SOI	350°C
Okojie et al. [9]	Piezoresistive pressure sensor	SiC	800°C
S. Koide et al. [10]	Hall effect sensor	AlGaN/GaN	400°C
Y. Zhu et al. [11]	Fiber-optic temperature sensor	Sapphire	1600°C
W.J. Pulliam et al. [12]	Fiber-optic pressure sensor	SiC	1100°C
This work	Pirani gauge	SiC	750°C

As for Pirani gauges, despite the fact that there are many excellent Pirani gauge designs, their performance at high temperatures and corrosive environments is a huge concern. As stated in the literature, Si-based electronics cannot operate at temperatures higher than 125°C [13]–[15]. Beyond this temperature, the minority carrier generation rate dramatically increases so the leakage current both in the device and in the circuitry becomes significant, which limits the operating temperature of the Si-based smart sensor. As the temperature goes beyond 125°C, the intrinsic carrier concentration will keep increasing and eventually reach the doping concentration, therefore the PN junction will not work. Additionally, when the temperature exceeds 500°C, silicon starts to show plastic deformation under mechanical stress. Beyond 800°C, Si will react with water and/or oxygen, resulting in the formation of an oxide layer on its surface. These properties make traditional Si-based devices show limited feasibility of applying to high-temperature environments. Although some of the microfabricated Pirani gauges reported in the literature are made of platinum [16], which is more compatible with high temperatures, the fabrication process shows less CMOS compatibility compared to common semiconductor-based devices and still would be limited by the maximum operating temperature of the Si electronics.

Silicon Carbide (SiC) is one of the most promising wide bandgap semiconductors for the development of integrated circuits and sensors intended for harsh environments. Compared to Si, SiC possesses a much wider bandgap, and it has a much lower intrinsic carrier concentration. As a result, SiC-based devices suffer less from leakage current and generation of minority carriers at elevated temperatures. For this reason, considerable effort has already been invested to develop SiC-based integrated circuits (ICs) aiming for high-temperature stability [17]–[19]. For instance, D.J. Spry *et al.* demonstrated a SiC IC with more than 100 transistors per chip which can work at 500°C for over 5000 hours [19].

SiC also has excellent mechanical properties. SiC is not only one of the hardest materials on earth, but it also has Young's modulus that ranges from 390 to 690 GPa while Si has Young's modulus of 160 GPa, therefore SiC is advantageous for the realization of suspended structures. Thanks to the strong covalent bond between silicon and carbon atoms (4.6 eV), SiC is highly chemically inert making it an excellent candidate for corrosive environment application. Pressure sensors for over-pressure monitoring based on poly-SiC with maximum operating temperature up to 800°C are reported in the literature [9], illustrating the prospect of SiC as a harsh environment compatible sensing material. It can be concluded that there is potential to incorporate high-temperature sensors with high-temperature readout electronics, eventually achieving harsh-environment compatible smart sensors.

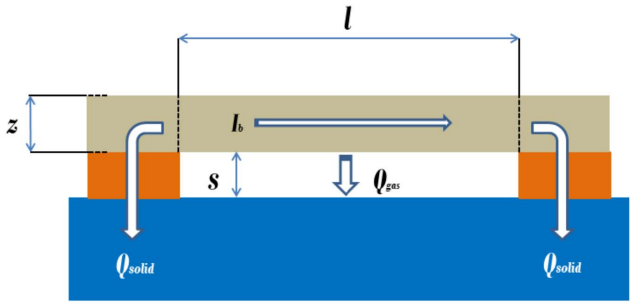

Fig. 1. Schematic illustration of a MEMS Pirani gauge. It consists of a suspended heating filament and two anchors to support the filament. This configuration allows to translate an amount of heat loss by the filament through the path Q_{gas} into a pressure.

This article presents the first poly-SiC based Pirani gauges, which is meant to achieve pressure monitoring at high temperatures. Surface micromachining is used as a starting point to enable future monolithic integration with SiC CMOS technologies. A modular design is one of the objectives, enabling tunable device performance, such as measurement range and sensitivity. Moreover, the device design is aimed to be independent from the substrate used, thus favoring its integration possibilities.

II. PHYSICS & ANALYTICAL MODELLING

The key component of a Pirani gauge is a suspended filament, of which the gaseous conduction of heat to its environment is affected by the ambient pressure (P). As shown in Fig. 1, a constant current is injected into the suspended thin filament. This causes its temperature to rise as a result of Joule heating. A temperature distribution will be developed over the filament after the system reaches the thermal equilibrium. Typically, the total heat losses (Q_{total}) consist of four parts: thermal convection ($Q_{convection}$), thermal radiation ($Q_{radiation}$), thermal conduction through the anchor parts (Q_{solid}) and through the gas (Q_{gas}). Among these terms, $Q_{radiation}$ and Q_{solid} are not related to pressure directly, so they are both treated as constants [20]. $Q_{convection}$ is negligible because no bulk movement of gas molecules exists at very low pressures [20]. Q_{gas} is the thermal conduction through the gas beneath the suspended filament and is the only heat loss source that is pressure-dependent.

The pressure dependency can be described by Knudsen number (K_n):

$$K_n = \frac{\lambda}{d} \tag{1}$$

Authorized licensed use limited to: TU Delft Library. Downloaded on January 12,2021 at 12:43:38 UTC from IEEE Xplore. Restrictions apply.

where λ is the mean free path of gas molecules which increases as pressure drops, and d is the characteristic length of a system, which in our case corresponds to the gap size. When $K_n < 0.01$, gas molecules will collide with each other intensively. In this condition, referred as continuum regime in fluid mechanics, Q_{gas} gets saturated and shows no sensitivity to pressure change.

As the pressure becomes lower, λ starts to increase and becomes comparable to the gap size. When $K_n > 1$, the sensor will enter the molecular regime, where Q_{gas} is linear to the number of molecules that participate in the gaseous conduction. If the pressure decreases, the number of molecules that participate in the gaseous conduction will decrease, causing a decrease in Q_{gas}. Therefore, the temperature of the suspended heater will increase until a new thermal equilibrium is reached. The pressure drop can be transduced into a resistance change of the filament employing the following equation:

$$R_{filament}(P) = R_0[1 + \alpha \bar{T}(P)] \tag{2}$$

where $R_{filament}(P)$ is the pressure-dependent resistance of the filament, and R_0 is the value of the resistance of the filament measured at standard atmospheric pressure at room temperature (usually 300 K). α is the temperature coefficient of resistance (TCR) of the filament material. $\bar{T}(P)$ is the average value of the temperature that exceeds the room temperature. From equation (2), it can be seen that the pressure-dependent average temperature change is needed to determine the filament resistance. $\bar{T}(P)$ is derived by Mastrangelo *et al.*, therefore $R_{filament}(P)$ can be further expressed as follows [1]:

$$R_{filament}(P) = R_0[1 + \frac{\delta\alpha}{\epsilon}(1 - \frac{tanh(\sqrt{\epsilon}\frac{l}{2})}{(\sqrt{\epsilon}\frac{l}{2})})] \tag{3}$$

in which,

$$\delta = \frac{I_b^2 R_0}{\lambda_b wlz}; \quad \epsilon = \frac{\eta\lambda_g(P)}{\lambda_b sz} - \frac{I_b^2 R_0}{\lambda_b wlz} \tag{4}$$

From the model, it can be seen that the dimensions (l, w, z, and s) of the Pirani gauge determine the sensor performance. The lower detection limit (P_L) is limited by the sum of $Q_{convection}$, $Q_{radiation}$ and Q_{solid}. At very low pressures, $Q_{convection}$, $Q_{radiation}$ and Q_{solid} will exceed Q_{gas}, and the device will lose sensitivity to the pressure below that point, despite of a large K_n. On the other hand, the higher detection limit (P_H) is limited by the saturation of Q_{gas} due to the decrease in the mean free path of gas molecules. In order to lower the P_L, the area of gaseous conduction should be increased by making the filament as long as possible. Besides, the anchor area should be kept as small as possible to minimize Q_{solid}. In such way, a large Q_{gas} / ($Q_{convection}$ + $Q_{radiation}$ + Q_{solid}) can be obtained thus achieving a lower P_L. In terms of P_H, the gap size should be minimized to make the saturation occur at a higher pressure. Generally, the most common ways to design a Pirani gauge with a large dynamic range are: (1) maximize the length of the filament; (2) minimize the gap distance between the filament and the substrate; (3) minimize the solid contact area. However, these design rules usually lead to a suspended filament with low stiffness.

TABLE II
THE DEFINITIONS OF THE VARIABLES IN ALL THE EQUATIONS

Symbol	Physical meaning
K_n	Knudsen number
λ	Mean free path of gas molecules
d	Characteristic length of a system
P	Pressure
$R_{filament}(P)$	Pressure-dependent resistance of the filament
R_0	Initial resistance of the filament
α	Temperature coefficient of resistance of filament material
$\bar{T}(P)$	Average value of the temperature that exceeds the environment temperature
l	Length
w	Width
z	Thickness
s	Gap size
λ_b	Thermal conductivity of SiC
η	Correction factor for the fringing heat flux
$\lambda_g(P)$	Thermal conductivity of air
I_b	Injected current
ρ	Material density
C_p	Heat capacity of the material
Q	Heat generation per unit volume of the medium
P_0	Transition pressure
λ_{g0}	Thermal conductivity of the air at a standard atmospheric pressure
T_a	Ambient pressure
v	Average velocity of gas molecules
$R_{fractional}(P)$	Fractional resistance change

As stated by Mitchell *et al.* [21] and Santagata *et al.* [22], long and thin suspended heaters are more vulnerable to deflection brought by external interferences. As a result, more heat is going to drain towards the substrate directly, and therefore the sensor will have a smaller dynamic range. In addition, putting the Pirani gauge in a high-temperature operating environment will amplify this effect because of the possible additional thermal buckling which can occur due to thermal expansion of the beam [23]. In order to overcome the buckling issue, researchers have tried different structures to improve the stiffness of long filament, for example, the ladder structure proposed by Mitchell *et al.* [21] and the tube-shaped Pirani gauge proposed by Santagata *et al.* [22].

In order to design a Pirani gauge that is capable to work in at elevated temperatures while showing high sensitivity over a large dynamic range, a MEMS Pirani gauge based on the micro-bridge structure in SiC is implemented. By the usage of poly-SiC, the stiffness of the structure can be greatly enhanced. This allows a longer and thinner Pirani gauge to be built even without dedicated supporting structures. Another advantage of SiC is that the tensile residual stress of the used poly-SiC layers results in flat (non-buckled) suspended beams and cancel out thermal expansion to some extent.

III. SIMULATION AND DESIGN

A finite element analysis (FEA) was implemented with COMSOL to verify the analytical model in section II. To simulate the operation of the Pirani gauge, the Joule Heating multiphysics interface which couples the "AC/DC" module and the "Heat Transfer" module was used. With the AC/DC module, an electrical current is injected to one end of the heater, and the other end is grounded. The resistivity at the

Authorized licensed use limited to: TU Delft Library. Downloaded on January 12,2021 at 12:43:38 UTC from IEEE Xplore. Restrictions apply.

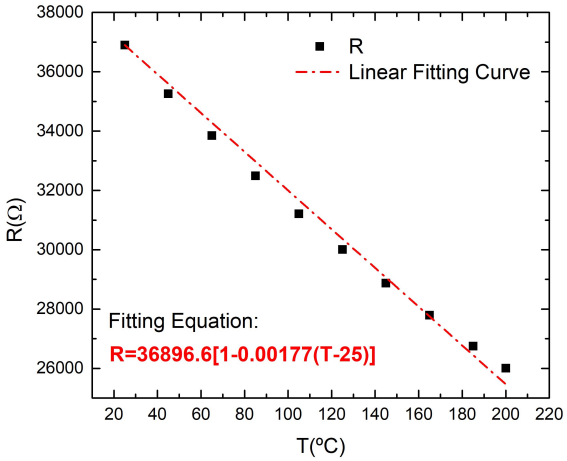

Fig. 2. The black dots show the TCR measurement result using the ELM structure, and the red line indicates the linear fitting result.

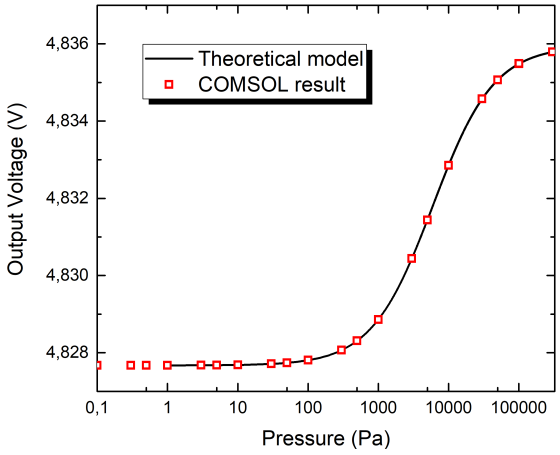

Fig. 3. A comparison between the analytical result and COMSOL simulation.

room temperature and the TCR of SiC are also required as inputs of this module to determine the temperature-dependent (thus the pressure-dependent) filament resistance. To do this, the resistance of an electrical linewidth measurement (ELM) structure was measured from room temperature to 200°C. The resistivity of the poly-SiC layer is $52.39 \times 10^{-3}\ \Omega \cdot$ cm. As indicated by the linear fit in Fig. 2, the poly-SiC layer obtained has a negative TCR of around -1770 ppm/°C in this temperature range.

In the Heat Transfer module, the temperature distribution on the filament (T) is defined by the following equation:

$$\rho C_p \cdot \nabla T = \frac{\partial}{\partial x}(\lambda \frac{\partial T}{\partial x}) + \frac{\partial}{\partial y}(\lambda \frac{\partial T}{\partial y}) + \frac{\partial}{\partial z}(\lambda \frac{\partial T}{\partial z}) + Q \quad (5)$$

where Q is the heat source. ρ, λ and C_p are density, thermal conductivity and heat capacity of the material respectively. For SiC, the corresponding values are 3210 kg/m^3, 370 W/(m·K) and 690 J/(kg·K). At both ends of the heating filament, the temperature is fixed at the ambient temperature (T_a), which serves as a boundary condition. An air block is inserted between the heater and substrate. The pressure-dependent thermal conductivity of the air $\lambda_g(P)$ is determined according to equation (6):

$$\lambda_g(P) = \lambda_{g0}[\frac{P/P_0}{1+(P/P_0)}]; \quad P_0 \approx \frac{\eta \lambda_{g0} w T_a}{(w+z)sv} \quad (6)$$

where λ_{g0} is the thermal conductivity of the air at a standard atmospheric pressure. P_0 is the empirical transition pressure. v is the average velocity of gas molecules. 20 pressure points from 0.1 Pa to 101 kPa were simulated.

The performance of a Pirani gauge ($l = 250\ \mu$m, $w = 8\ \mu$m, $z = 2\ \mu$m and $s = 2\ \mu$m, with 600 μA biasing current) is predicted by both the theoretical model and the COMSOL model mentioned above. As shown in Fig. 3, the results obtained from FEA simulation overlap exactly to the curve predicted by the analytical model. It can, therefore, be concluded that FEA is in agreement with the analytical model.

Tab. II summarizes geometries of Pirani gauges that were fabricated. As shown in the table, multiple combinations of length, width, and gap size are taken into consideration. In this study, the thickness of the heating filament is kept constant to 2 μm. As predicted by the analytical model, different geometries would result in different sensor performance such as dynamic range and sensitivity. Therefore, the possibility of integrating two or more Pirani gauges with different geometries into a single chip would allow us to expand the measurement range. The effect brought by different dimensional parameters can be verified at the measurement stage.

TABLE III
DIMENSIONAL PARAMETERS OF THE FABRICATED PIRANI GAUGES

Length (μm)	Width (μm)	Gap size (μm)
250	8	0.5
250	8	1
250	8	2
250	6	2
250	10	2
250	12	2
150	8	2
500	8	2
1000	8	2

IV. FABRICATION

The process flow of the Pirani gauge is summarized in Fig. 4. Only three photolithographic steps are needed to fabricate the device. Surface micromachining was used to create the suspended heating filaments. First, a 300 nm Si_3N_4 layer was deposited on the silicon substrate by LPCVD with a gas mixture of dichlorosilane ($SiCl_2H_2$) and ammonia (NH_3) at 850°C and 20 Pa (Fig. 4a). This layer serves as an additional electrical isolation layer between the metal and the Si substrate, and was patterned with the same mask that will be then used for the metal layer (Fig. 4b). On the front side of the substrate, TEOS (tetraethyl orthosilicate) oxide was coated by means of plasma enhanced chemical vapor deposition (PECVD) (Fig. 4c). This oxide layer is not only a sacrificial layer for the release of the suspended heating filament (microbridge) but also an electrical and thermal isolation layer. The thickness of the oxide defines the gap size of the Pirani gauge. 0.5 μm, 1 μm, and 2 μm oxide layer were deposited on separate batches. After the oxide deposition, a poly-SiC layer of 2000 nm was deposited with $SiCl_2H_2$ (dichlorosilane), C_2H_2 (acetylene) as precursor gases, and was in-situ doped

Authorized licensed use limited to: TU Delft Library. Downloaded on January 12,2021 at 12:43:38 UTC from IEEE Xplore. Restrictions apply.

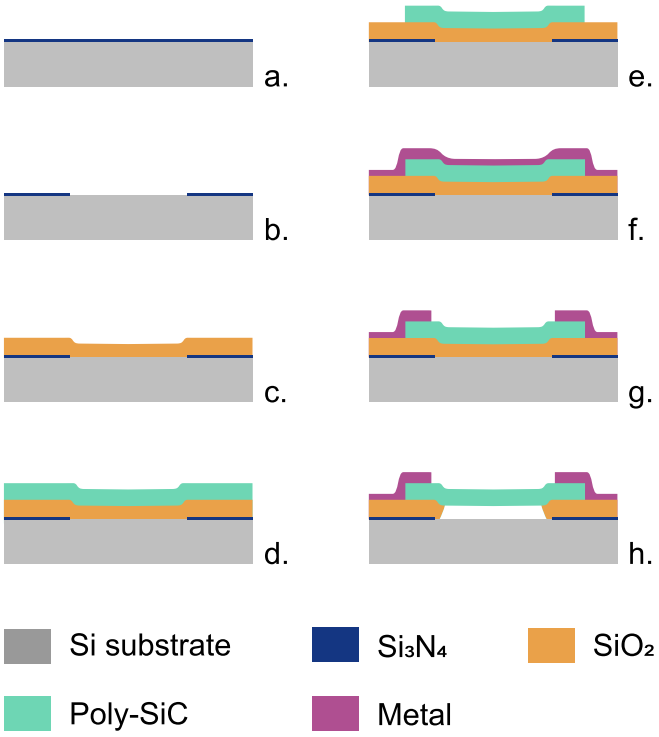

Fig. 4. Schematic illustration of the process steps for the fabrication of the SiC-based Pirani gauge. (a) LPCVD of Si3N4 layer; (b) Patterning of Si3N4 layer; (c) Deposition of SiO2 sacrificial layer; (d) Poly-SiC deposition; (e) Poly-SiC patterning; (f) Sputtering of metal layer; (g) Metal layer patterning; (h) Release of the poly-SiC structure.

with NH_3 at 860°C and 80 Pa (Fig. 4d). More information on the poly-SiC deposition process can be found in [24]. The deposited carbide layer has a tensile stress of 403.9 MPa, which is within the specification comparing to the result obtained by Bruno *et al.* Subsequently, a patterning step was conducted to define the suspended micro-bridge structure and the anchor area (Fig. 4e).

Then, a metal layer was sputtered (Fig. 4f) and patterned (Fig. 4g) to form the metal lines and pads for electrical measurement. Aluminum (Al) and titanium (Ti) were used as metallization materials. Earlier research showed that these metals will form an ohmic contact to the doped poly-SiC layers employed in this work [5], [25], [26]. A post-deposition annealing process in a nitrogen environment was followed to relieve the strain and improve the contact property at the metal-semiconductor interface. Finally, the sacrificial oxide layer was etched away to release the micro-bridge (Fig. 4h). In order to avoid any stiction caused by the capillary forces during a wet releasing step, vapor HF was used.

The longest Pirani gauge that was fabricated had a length of 1000 μm. Although this geometry is in principle most likely to show the highest deflection between the different designs, it can be seen from Fig. 5 that the realized 1000 μm does not show any deflection after realization.

V. Results and Discussion

A. Measurement Setup

A dedicated measurement setup for calibrating Pirani gauges is built as shown in Fig. 6. The setup is able to provide

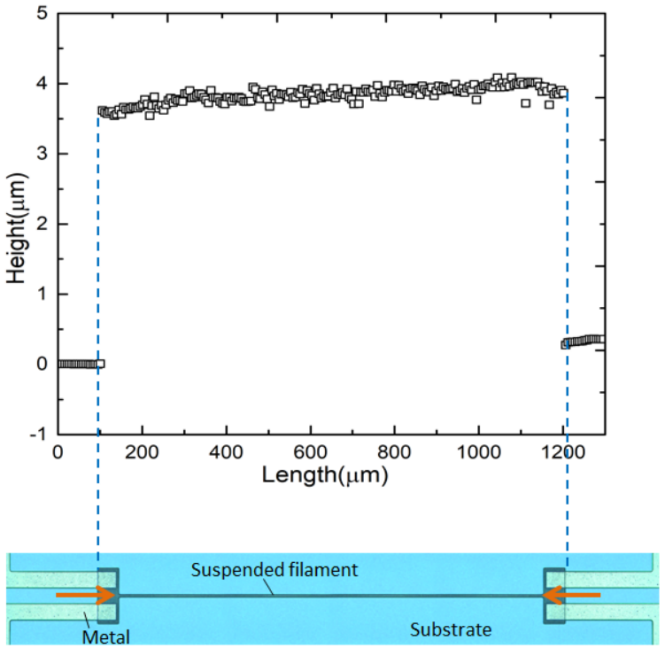

Fig. 5. Distance between the top surface of the micro-bridge and Si substrate along the beam. The orange arrows indicate the position of the cross-section.

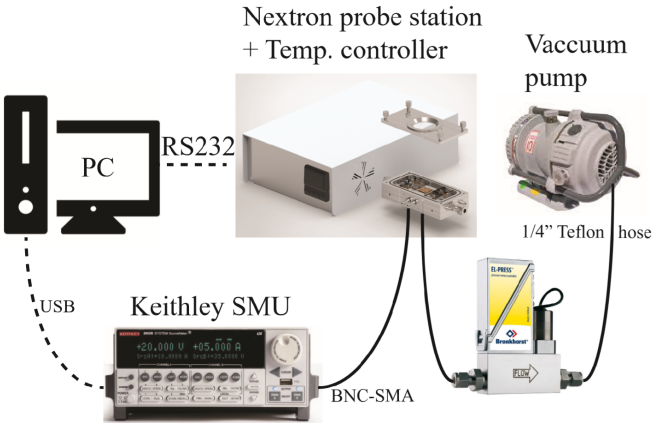

Fig. 6. Measurement setup used for calibration [27]. The setup contains a MPS, a mass flow controller, a temperature controller and a vacuum pump.

a low-pressure environment with values ranging from 10 Pa to atmospheric pressure. The controller of this setup can change the pressure in steps of 500 Pa while the internal pressure sensor has a resolution of 10 Pa. The micro-fabricated Pirani gauges are calibrated by using the pressure values from the internal pressure gauge.

The setup also contains a microprobe station (MPS) which is equipped with four-probe needles. These probe needles are connected to a source meter (Keithley 2612B) to measure the resistance of Pirani gauges. A hotplate is also integrated with the probe station and is able to create a hot surface up to 750 °C.

When calibrating a Pirani gauge, the device is put in the MPS where a certain vacuum is created. Below 20 kPa, the pressure increment was 500 Pa, because the sensitivity of the realized gauges is larger in this pressure regime.

Authorized licensed use limited to: TU Delft Library. Downloaded on January 12,2021 at 12:43:38 UTC from IEEE Xplore. Restrictions apply.

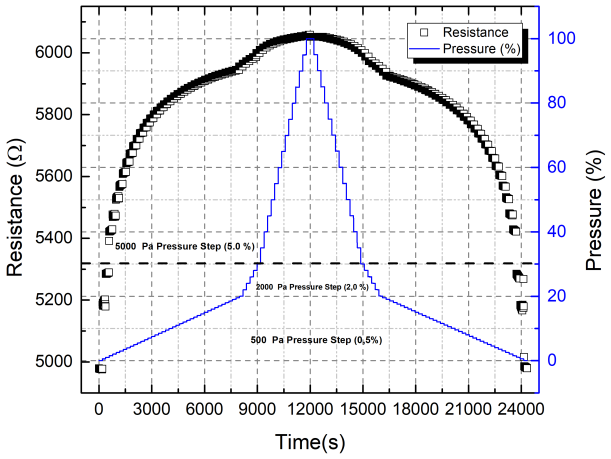

Fig. 7. The pressure profile for the calibration (blue curve) and the output voltage of the reference Pirani gauge as a function of pressure (black dots).

As for 20-30 kPa and 30-100 kPa, the pressure step was set as 2000 Pa and 5000 Pa respectively. In total, there were 60 pressure set-points used for calibration. For each of the points, the measurement was paused for 200 s so that the pressure in the micro-chamber can fully stabilize whereafter the electrical measurement is performed. The pressure profile for calibration is shown by the blue curve in Fig. 7.

B. Dimensioning of the Pirani Gauge

As stated in Mastrangelo's model, dimensional parameters play a significant role in the performance of the sensor. To study the effect of the variation in the geometry on the performance, a Pirani gauge with a length of 250 μm, a width of 8 μm, a thickness of 2 μm and a gap size of 2 μm is taken as a reference device. The performance of the reference gauge was measured and was compared to the performance of gauges with other dimensions. The reference device was biased with a constant current of 600 μA. The calibration curve of the reference device is plotted in Fig. 7. The gauge resistance ranges from 4978.3 Ω to 6060.0 Ω from the lowest pressure set-point of 10 Pa up to 100 kPa, which corresponds to a maximum resistance deviation of 17.8 %. The Pirani gauge shows a response to the pressure change without hysteresis, as indicated by the symmetrical shape of the calibration curve in Fig. 7. The performances of the gauges with other dimensions are demonstrated in Fig. 8. In this figure, the scattered data points are obtained with the measurement setup, and the continuous curves are fitting curves based on equation (3) according to the experimental data. From the fitting data, the reference gauge has the highest sensitivity of 0.47 Ω/Pa at around 10 Pa.

Fig. 8a shows the performance of gauges with different lengths. Since Pirani gauges with various dimensions have different initial resistance, the output resistance is expressed with the factional resistance change $R_{fractional}(P)$ as shown in equation (7). With increasing length, the calibration curve shifts towards the left because Q_{gas} takes a larger proportion in the total heat transfer. As a result, the longer gauge has

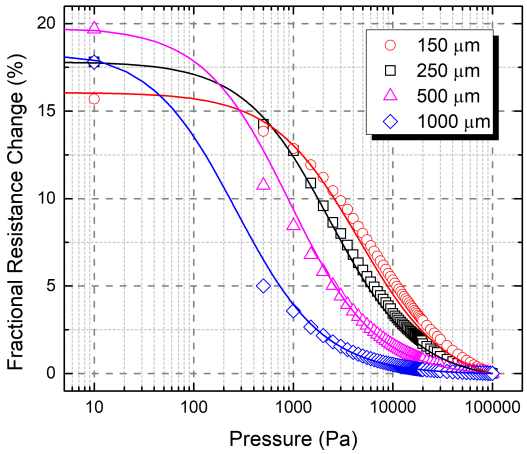

(a)

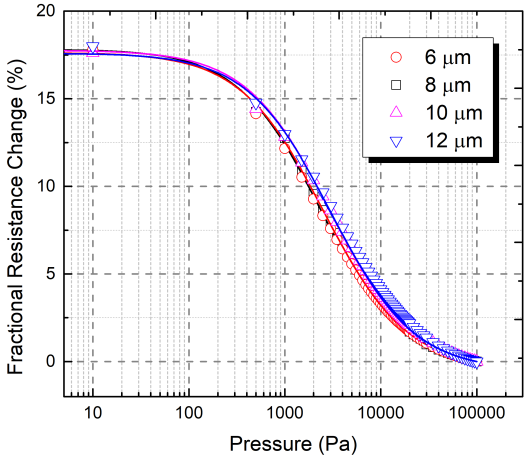

(b)

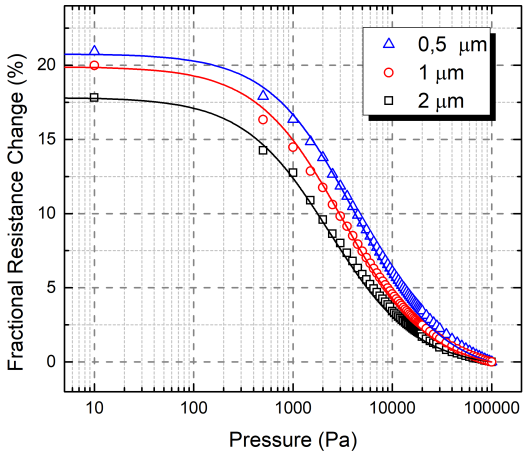

(c)

Fig. 8. The calibration curves for device with different (a) lengths; (b) widths; (c) gap sizes comparing to the reference device. The scattered points represent experimental data, while continuous curves represent fitted data.

a smaller P_L. From 150 μm to 1000 μm, the maximum sensitivity increases from 0.13 Ω/Pa to 16.76 Ω/Pa. It is worth noting that the maximum sensitivity of each gauge locates at 10 Pa, which implies that the gauge is still sensitive below

Authorized licensed use limited to: TU Delft Library. Downloaded on January 12,2021 at 12:43:38 UTC from IEEE Xplore. Restrictions apply.

10 Pa.

$$R_{fractional}(P) = \frac{R_0 - R_{filament}(P)}{R_0} \times 100\% \qquad (7)$$

Fig. 8b shows the impact of the width variations. The reduction of the heater width only causes a slight left shift of the calibration curve. Despite a larger width increases Q_{gas}, the solid contact between the filament and the anchor region also increases with the width, causing Q_{solid} to increase with the same order. Therefore, the dynamic range of gauges with different width does not vary too much. However, due to the increase in the heat exchange surface, the wider gauge is less power-efficient. For example, the narrowest gauge ($w = 6\ \mu$m) and the widest gauge ($w = 12\ \mu$m) have initial resistances of 8591.5 Ω and 3771.1 Ω, and are biased with a current of 424 μA and 965 μA respectively. As shown in Fig. 8b, both of them have a similar fractional resistance change of around 17.8 %, while the narrowest gauge consumes 56.2 % less power than the widest gauge.

Devices with different gap sizes (0.5 μm, 1 μm, and 2 μm) were measured. As can be seen from Fig. 8c, the device with a smaller gap (blue curve) tends to saturate at a higher pressure. In general, the experimental results align with the prediction of the analytical model qualitatively: longer beam will have larger sensitivity in low pressure range, and the gauge with smaller air gap has larger sensitivity near the standard atmospheric pressure. However, numerically, the experimental results do not match the analytical results. From the measurement, the reference gauge shows a 17.8 % fractional resistance change, while the analytical model and COMSOL simulation both predict only 0.16 % of fractional resistance change. The reason for the discrepancy could be that the material properties of poly-SiC reported in the literature which used as inputs of the analytical model, such as thermal conductivity, are different from the material properties of SiC we deposited.

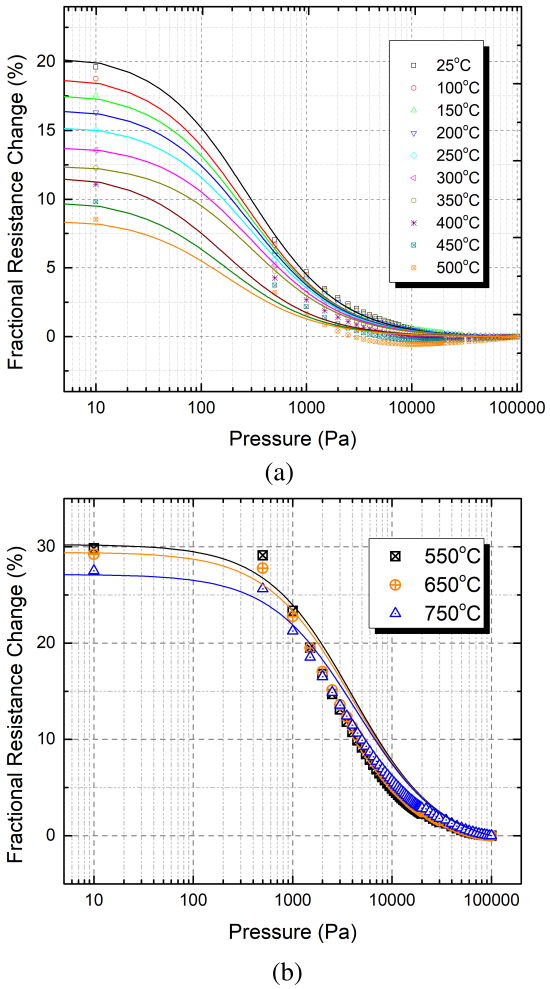

Fig. 9. The calibration curve of devices ($l = 1000\ \mu$m, $w = 8\ \mu$m, $z = 2\ \mu$m and $s = 2\ \mu$m) (a) with Al pads from 25°C to 500°C; (b) with Ti pads from 550, 650 and 750°C. The sensitivity decreases as temperature rises. The scattered points represent experimental data, while continuous curves represent fitted data.

C. High-Temperature Characterization

The micro-fabricated Pirani gauges were characterized at different temperatures to examine the high-temperature performance. The longest Pirani gauge (1000 μm) was used for the test because it is most likely to experience a buckling among all the geometries. First, the Pirani gauges with conventional Al metallization was measured. The measurement was carried out from 25°C to 500°C in steps of 50°C. The calibration curves are plotted in Fig. 9a. As the temperature increases, the fractional resistance change reduces and the maximum sensitivity decreases from 17.63 Ω/Pa at 25°C to 6.15 Ω/Pa at 500°C, which results from the decrease in the material TCR at an elevated temperature.

For characterization beyond 500°C, the realized devices with Ti metallization were measured. The reason for this is the higher melting point of Ti of 1668°C compared to 575°C for Al with 1 % Si. Additionally, Ti has a work function of 4.33 eV, which is similar to Al (4.06-4.26 eV). As reported in [25], [26], Ti is able to form an Ohmic contact with SiC and is less reactive and more compatible with high-temperature environments. The measurement results at 550, 650, and 750°C are given in Fig. 9b. Even at these temperatures, the device demonstrates a repeatable response to pressure change. The maximum sensitivity can still be obtained at 10 Pa, which is 1.35 Ω/Pa at 550°C, 1.23 Ω/Pa at 650°C, and 0.81 Ω/Pa at 750°C. To the best of authors' knowledge, this is the first time that the operating temperature of the Pirani gauge has been pushed to such a high temperature.

VI. Conclusion

This work reports on the realization of a CMOS compatible vacuum gauge operating at elevated temperatures. A MEMS Pirani gauge in SiC is fabricated with surface micro-machining technique by means of a three-mask process. The use of SiC combines favorable properties such as a useful TCR, high mechanical stiffness, and compatibility with high temperatures and harsh environments. The realized Pirani gauges can achieve a length of 1000 μm without any mechanical supporting structure to prevent buckling. At room temperature, the gauge with reference geometry showed a maximum sensitivity of 0.47 Ω/Pa and a fractional resistance change of 17.8 %. High-temperature characterization on the 1000 μm long beam revealed the desired operation even

Authorized licensed use limited to: TU Delft Library. Downloaded on January 12,2021 at 12:43:38 UTC from IEEE Xplore. Restrictions apply.

up to a maximum temperature of 750°C, with a maximum sensitivity of 0.81 Ω/Pa. These results further illustrate the potential of poly-SiC Pirani gauges for applications at high temperatures and in harsh environments. However, at 750°C, the filament resistance of some devices increased while the pressure was decreasing. The future work will include a closer investigation into the undesired device performance beyond 750°C. In such an analysis the temperature dependency of the TCR, the possible buckling and radiative losses at high temperatures need carefully to be taken into account.

The future outlook of this work is to be integrated with state of the art SiC CMOS technologies to achieve an all-SiC monolithically integrated MEMS + ASIC platform. In order to achieve this, the process flow of this poly-SiC MEMS sensor should be integrated into the back-end of line processing of the SiC CMOS process, where thermal budget, metallization, contamination and passivation aspects need to be considered.

REFERENCES

[1] C. H. Mastrangelo and R. S. Müller, "Microfabricated thermal absolute-pressure sensor with on-chip digital front-end processor," *IEEE J. Solid-State Circuits*, vol. 26, no. 12, pp. 1998–2007, Dec. 1991.

[2] F. Santagata, J. F. Creemer, E. Iervolino, L. Mele, A. W. van Herwaarden, and P. M. Sarro, "A tube-shaped buried pirani gauge for low detection limit with small footprint," *J. Microelectromech. Syst.*, vol. 20, no. 3, pp. 676–684, Jun. 2011.

[3] F. Yu and J. Zhang, "Single-walled carbon nanotube pirani gauges prepared by DEP assembly," *IEEE Trans. Nanotechnol.*, vol. 12, no. 3, pp. 323–329, May 2013.

[4] J. Romijn *et al.*, "A miniaturized low power pirani pressure sensor based on suspended graphene," in *Proc. IEEE 13th Annu. Int. Conf. Nano/Micro Eng. Mol. Syst. (NEMS)*, Apr. 2018, pp. 11–14.

[5] T. Kimoto and J. A. Cooper, *Fundamentals of Silicon Carbide Technology: Growth, Characterization, Devices and Applications*. New York, NY, USA: Wiley, 2014.

[6] D. J. Young, J. Du, C. A. Zorman, and W. H. Ko, "High-temperature single-crystal 3C-SiC capacitive pressure sensor," *IEEE Sensors J.*, vol. 4, no. 4, pp. 464–470, Aug. 2004.

[7] M. Werner, O. Dorsch, and E. Obermeier, "High-temperature pressure sensor using p-type diamond piezoresistors," *Diamond Rel. Mater.*, vol. 4, nos. 5–6, pp. 873–876, May 1995.

[8] S. Li, T. Liang, W. Wang, Y. Hong, T. Zheng, and J. Xiong, "A novel SOI pressure sensor for high temperature application," *J. Semicond.*, vol. 36, no. 1, Jan. 2015, Art. no. 014014.

[9] R. S. Okojie, D. Lukco, V. Nguyen, and E. Savrun, "4H-SiC piezoresistive pressure sensors at 800 °C with observed sensitivity recovery," *IEEE Electron Device Lett.*, vol. 36, no. 2, pp. 174–176, Feb. 2015.

[10] S. Koide, H. Takahashi, A. Abderrahmane, I. Shibasaki, and A. Sandhu, "High temperature Hall sensors using AlGaN/GaN HEMT structures," in *Proc. J. Phys., Conf.*, vol. 352, Mar. 2012, Art. no. 012009.

[11] Y. Zhu, Z. Huang, F. Shen, and A. Wang, "Sapphire-fiber-based white-light interferometric sensor for high-temperature measurements," *Opt. Lett.*, vol. 30, vol. 7, pp. 711–713, Apr. 2005.

[12] W. J. Pulliam *et al.*, "Micromachined SiC fiber optic pressure sensors for high-temperature aerospace applications," in *Industrial Sensing Systems*. Boston, MA, USA: SPIE Press, 2000, pp. 21–30.

[13] G. H. Kroetz, M. H. Eickhoff, and H. Moeller, "Silicon compatible materials for harsh environment sensors," *Sens. Actuators A, Phys.*, vol. 74, nos. 1–3, pp. 182–189, Apr. 1999.

[14] P. French, G. Krijnen, and F. Roozeboom, "Precision in harsh environments," *Microsyst. Nanoeng.*, vol. 2, no. 1, pp. 1–12, Oct. 2016.

[15] P. G. Neudeck, R. S. Okojie, and L.-Y. Chen, "High-temperature electronics—A role for wide bandgap semiconductors?" *Proc. IEEE*, vol. 90, no. 6, pp. 1065–1076, Jun. 2002.

[16] J. Claudel *et al.*, "High resolution nano-gap pirani sensor for pressure measurement in wide dynamic range operation around atmospheric pressure," in *Proc. 30th Anniversary Eurosensors Conf. (Eurosensors)*, Budapest, Hungary, Sep. 2016, vol. 168, Jan. 2016, pp. 798–801.

[17] R. Ghandi *et al.*, "Silicon carbide integrated circuits with stable operation over a wide temperature range," *IEEE Electron Device Lett.*, vol. 35, no. 12, pp. 1206–1208, Dec. 2014.

[18] N. Kuhns *et al.*, "Complex high-temperature CMOS silicon carbide digital circuit designs," *IEEE Trans. Device Mater. Rel.*, vol. 16, no. 2, pp. 105–111, Jun. 2016.

[19] D. J. Spry *et al.*, "Prolonged 500 °C operation of 100+ transistor silicon carbide integrated circuits," *Mater. Sci. Forum*, vol. 924, pp. 949–952, Jun. 2018.

[20] J. C, B. H. Stark, and K. Najafi, "A micromachined pirani gauge with dual heat sinks," *IEEE Trans. Adv. Packag.*, vol. 28, no. 4, pp. 619–625, Nov. 2005.

[21] J. Mitchell, G. R. Lahiji, and K. Najafi, "An improved performance poly-Si pirani vacuum gauge using heat-distributing structural supports," *J. Microelectromech. Syst.*, vol. 17, no. 1, pp. 93–102, Feb. 2008.

[22] F. Santagata, "Mechanical Robustness and Hermeticity Monitoring for MEMS Thin Film Encapsulation," Ph.D. dissertation, Univ. Technol. Delft, Delft, The Netherlands, 2011.

[23] M. Chiao and L. Lin, "Self-buckling of micromachined beams under resistive heating," *J. Microelectromech. Syst.*, vol. 9, no. 1, pp. 146–151, Mar. 2000.

[24] B. Morana *et al.*, "A silicon carbide MEMS microhotplate for nanomaterial characterization in TEM," in *Proc. IEEE 24th Int. Conf. Micro Electro Mech. Syst.*, Cancun, Mexico, Jan. 2011, pp. 380–383.

[25] T. Dinh, N. T. Nguyen, and D. V. Dao, *Thermoelectrical Effect in SiC for High-Temperature MEMS Sensors*. New York, NY, USA: Springer, 2018.

[26] L. Huang *et al.*, "Low resistance Ti ohmic contacts to 4H-SiC by reducing barrier heights without high temperature annealing," *Appl. Phys. Lett.*, vol. 100, no. 26, Jun. 2012, Art. no. 263503.

[27] L. M. Middelburg, H. W. van Zeijl, S. Vollebregt, B. Morana, and G. Q. Zhang, "Toward a self-sensing piezoresistive pressure sensor for all-SiC monolithic integration," *IEEE Sensors J.*, early access, Jun. 1, 2020, doi: 10.1109/JSEN.2020.2998915.

Jiarui Mo received the bachelor's degree in measuring and testing technology & instruments from Chongqing University and the master's degree in electrical engineering from the Delft University of Technology in 2019. He is currently pursuing the Ph.D. degree with the Department of Electronic Components, Technology and Materials (ECTM), Delft University of Technology. His current research interests include harsh environment sensing and the monolithic integration of SiC devices.

Luke M. Middelburg (Member, IEEE) received the B.Sc. degree in electrical engineering and the M.Sc. degree in microelectronics from the Delft University of Technology in 2014 and 2016, respectively. He is currently pursuing the Ph.D. degree with the Department of Electronic Components, Technology and Materials (ECTM), Delft University of Technology. Previous research involves the application of impedance spectroscopy for Particulate Matter (PM) sensing and for the development of a fuel sensor to determine the composition of bio-ethanol containing fuel mixtures, both in collaboration with Ford Motor Company, USA. He has coauthored seven journal publications, ten conference proceedings, two book chapters, and two patent applications. His current research interests include the exploitation of non-linear effects in MEMS accelerometers and the development of silicon carbide (SiC)-based sensors. Additionally, the monolithic integration of SiC CMOS front-end read-out electronics is studied, yielding a harsh environment compatible sensing platform. This project is funded by the European Consortium project "IoSense."

Authorized licensed use limited to: TU Delft Library. Downloaded on January 12,2021 at 12:43:38 UTC from IEEE Xplore. Restrictions apply.

Bruno Morana received the M.Sc. degree in electronic engineering from the Polytechnic of Milan, Milan, Italy, in 2007. He is currently pursuing the Ph.D. degree with the Laboratory of Electronic Components Technology and Materials, Delft University of Technology, with a focus on the fabrication of surface micromachined nanoreactors made of silicon carbide. During the master's thesis, he joined the Electronic Technology Department, Polytechnic University of Madrid, Madrid, Spain, where he was a Researcher. His master's thesis and research activity focused on the fabrication and characterization of Si and SiGe nanocrystals embedded in SiO_2 thin films. In 2008, he joined the Laboratory of Electronic Components Technology and Materials, Delft University of Technology, Delft, The Netherlands, as a Researcher. He focused on the development and optimization of procedures for the ultra-high vacuum compatible assembly of MEMS nanoreactors. His research interests include the fabrication and characterization of thin films and the development of fabrication technologies for MEMS devices.

H. W. van Zeijl (Member, IEEE) was born in Wateringen, The Netherlands, in 1958. He received the Engineering Diploma degree in technical physics from the Technical College in Rijswijk in 1981 and the Ph.D. degree from the Delft University of Technology, The Netherlands, in 2005, based on research on bipolar transistors with self-aligned emitter-base metallization and back-wafer-aligned collector contacts. In 1981, he joined the Interuniversity Reactor Institute, Delft, where he worked in neutron diffraction and instrumental neutron activation analysis. In 1986, he joined the Delft Institute of Microelectronics and Submicron Technology (DIMES), Delft University of Technology. From 1989 to 1998, he was responsible for the mask fabrication and lithography in the DIMES IC process research sector. He developed several technology courses, a full week training for engineers from relevant fields in the industry and academia. These courses are held for more than 40 times and are also given at Universities in China (Beijing, Shanghai, and Chengdu) and at companies (CNS and SHTP) in Vietnam (Ho Chi Minh). Besides these educational activities, he cooperated in different research project related to Lithography, MEMs, 3D integration, and Packaging and Solid State Lighting Integration. Since August 2017, he has been a Staff Member with the Laboratory of Electronic Components Materials and Technology (ECTM). He has coauthored more than 80 technical articles and several patents.

Sten Vollebregt (Senior Member, IEEE) received the B.Sc. and M.Sc. *(cum laude)* degrees in electrical engineering from the Delft University of Technology in 2006 and 2009, respectively, and the Ph.D. degree from the Microelectronics Department, Delft University of Technology, in 2014, on the low-temperature high-density growth of carbon nanotubes for application as vertical interconnects in 3D monolithic integrated circuits. For his master's thesis, he investigated the growth of carbon nanotubes at the NanoLab, Newton, MA, USA, and AIXTRON, Cambridge, U.K.

After obtaining his Ph.D., he held a postdoctoral position on the wafer-scale integration of graphene for sensing applications together with the Faculty of Mechanical Engineering and several industrial partners. During this research, he developed a unique transfer-free wafer-scale CVD graphene process. Since October 2017, he has been an Assistant Professor with the Laboratory of Electronic Components, Technology and Materials, Delft University of Technology, where his research focuses on the integration of emerging electronic materials into semiconductor technology for sensing applications. He has coauthored more than 25 journal publications, four book chapters, and holds three patents. His research interests include (carbon-based) nanomaterials, 3D monolithic integration, wide-bandgap semiconductors, and (harsh) environmental sensors.

Guoqi Zhang (Fellow, IEEE) received the Ph.D. degree from the Delft University of Technology, The Netherlands, in 1993. He has worked for NXP Semiconductors as the Senior Director of Technology Strategy until 2009 and as a Philips Research Fellow until May 2013. He serves as the Deputy Director for the European Center for Micro- and Nanoreliability (EUCEMAN); also the Co-Chair for the Advisory Board of International Solid State Lighting Alliance (ISA); and also a Secretary General for the International Technology Roadmap of Wide bandgap Semiconductors (ITRW). He is currently a Chair Professor of the Institute of Micro/Nanoelectronics System Integration and Reliability, Delft University of Technology. He has authored or coauthored more than 400 scientific publications. His research interests include multi-level heterogeneous system integration and packaging, wide band gap semiconductors sensors and components, multi-physics and multiscale modeling of micro/nanoelectronics, and digital twin for mission critical multifunctional electronics components and systems.

Authorized licensed use limited to: TU Delft Library. Downloaded on January 12,2021 at 12:43:38 UTC from IEEE Xplore. Restrictions apply.